Appl. Phys. B 39, 251–259 (1986)

Applied Physics B Photophysics and Laser Chemistry

Doppler Effects due to Thermal Macromotion of Ions in an rf Quadrupole Trap

L. S. Cutler, C. A. Flory, R. P. Giffard, and M. D. McGuire
Hewlett-Packard Laboratories, Palo Alto, CA 94303, USA

Received 30 July 1985/Accepted 20 November 1985

Abstract. The second-order Doppler shift is an important source of systematic error in rf quadrupole trapped ion frequency standards. This shift can be reduced by cooling the secular motion of the ion cloud with a light background gas at low pressure. Using a thermalized ion cloud model, it is possible to relate the Doppler shift to the temperature of the ion cloud. It is shown that, in practice, the measured frequency of the first-order Doppler sidebands can be used to determine the ion cloud temperature.

PACS: 35, 32

The technique of ion confinement using an rf quadrupole trap [1–3] has been used to good effect in several different types of physical experiments. For example, the selectivity of the trapping process provides a means of mass spectroscopy. The comparatively long, collision-free ion storage time has also made possible measurements of such phenomena as small scattering cross-sections and weak optical transitions. In particular, extremely high precision microwave hyperfine spectroscopy [4, 5] has been carried out, leading to the development of a new type of atomic frequency standard [6–10].

In an rf trap the confined ions experience a small amplitude oscillation (micromotion) driven by the non-uniform, time-varying field. This motion produces an effective trapping potential in which the ions execute comparatively large thermally excited periodic orbits. The overall motion of the trapped ions causes a shift of the average hyperfine transition frequency due to the second-order Doppler effect of special relativity. It has been argued [7, 10] that this shift is the most significant absolute offset in a trapped ion frequency standard, and must be stabilized and accounted for to achieve the desired stability and accuracy.

It has been demonstrated [2, 10, 12, 13] that the introduction of a low pressure of a light background gas reduces the amplitude of the macromotion of heavy ions, decreasing the total second-order Doppler shift. Under these conditions one can use as a model a cloud of ions in which individual ion macromotion is thermalized in the effective trapping potential modified by the space charge of the rest of the ions. For a given macromotion temperature the distribution of ions within the cloud can be obtained by solving a set of self-consistent equations [14, 15]. The ion distribution, and the associated distribution of macromotion orbits, can then be used to calculate the total second-order Doppler shift due to both micromotion and macromotion. Thus if the number of ions, the trapping parameters, and the macromotion temperature are known, the second-order Doppler shift can be calculated.

The macromotion temperature of a trapped ion cloud will depend, in general, on the balance of heating effects resulting from collisions and irregularities in the trapping potentials, and cooling due to collisions with any background gas which may be present [2]. In practice, neither the heating rate nor the cooling rate is accurately predictable, and it is necessary to devise some method of measuring the ion macromotion temperature.

The purpose of this paper is to show how one can accurately determine the temperature of a trapped ion cloud by measuring the first-order Doppler sidebands of the microwave hyperfine resonance. The theory developed is found to corroborate previous experimental evidence [10, 13] of the self-consistency of the thermalized cloud model used. The basic idea is as

follows. Due to their thermal energy, trapped ions move in periodic orbits which are determined by the total effective potential. When these ions are irradiated with a traveling electromagnetic wave, their periodic motion causes the ions to see a signal which is phase modulated at the motional frequency by the first-order Doppler shift. A signal with periodic phase modulation has a spectral density comprised of an unshifted carrier and sidebands uniformly spaced by the modulation frequency. Thus, the average spectral density that the ion cloud sees is a narrow unshifted carrier with first-order Doppler sidebands that are smeared by the velocity and trajectory distributions of the ion thermal macromotion. The first-order Doppler spectrum of confined atoms was first discussed by Dicke [16], and such sideband spectra have recently been observed in trapped mercury ion frequency standards [13, 17].

In the following sections we show how the sideband spectral density may be calculated for a given macromotion temperature on the assumption of a thermalized ion cloud. These results are then compared with spectral densities observed in a ^{199}Hg frequency standard [13] in order to determine the macromotion temperature. As will be shown, the model accurately reproduces the observed spectral densities corroborating the assumption of a thermalized ion cloud and clearly determining the temperature required to compute the second-order Doppler shift of the frequency standard.

Jardino et al. [17] have recently calculated first-order Doppler spectral densities for trapped mercury 199 ions using the same theoretical method. Their results are compared with experiments in which space charge effects are not dominant. Under those given conditions they show that the frequency of the first-order Doppler sidebands does not vary with temperature. Our investigation concentrates on the space-charge-dominated situation with known, constant, ion population, as appropriate in our experiments with helium cooling gas. Under these circumstances we find that the sideband frequency can be used to obtain an accurate measure of the ion macromotion temperature. It will be shown that these results are not at variance with those of [17].

1. Theoretical Description of Ion Thermal Macromotion in a Spherical Pseudopotential

A single ion in an rf quadrupole trap feels a time-averaged force generated by its motion in superposed oscillating and static electric fields. The instantaneous electric potential seen by the ion is given in cylindrical coordinates by

$$\phi(t) = [U - V\cos(\Omega t)]\,(\varrho^2 - 2z^2)/\xi^2\,, \tag{1}$$

where U and V are the dc and rf voltages applied, Ω is the rf frequency, and ξ is a dimensional parameter characterizing the trap electrodes. It is well known that the net effect of the oscillating part of the field is to create a harmonic restoring force on an ion, provided the displacement during an rf cycle is small compared to the distance from the trap center. This is equivalent to a cylindrically symmetric pseudopotential $\Psi(\varrho, z)$ given by

$$\Psi(\varrho, z) = \left(\frac{q^2V^2}{m\Omega^2\xi^4}\right)(\varrho^2 + 4z^2)\,, \tag{2}$$

where q and m are the charge and mass of the trapped ion. The superposition of the field due to the dc voltage U and the pseudopotential Ψ from the rf voltage gives an effective potential $\Phi(\varrho, z)$. It is possible to choose the parameters U, V, and Ω to give a spherically symmetric effective potential, which in spherical coordinates is

$$\Phi(\mathbf{r}) = \left(\frac{m\omega^2}{2}\right)r^2\,, \tag{3}$$

where

$$\omega \equiv 2qV/m\Omega\xi^2\,.$$

Since the use of spherical symmetry greatly simplifies the calculations and the observations to be discussed were made with an almost spherical effective potential, this is the case which will be analyzed. A single ion would undergo three-dimensional simple harmonic motion in effective potential (3) at a characteristic macromotion frequency ω. Superposed on this motion is a small amplitude driven micromotion oscillation at frequency Ω. It is easily shown that the mean square velocity $\langle v^2\rangle$ of this micromotion is

$$\langle v^2\rangle = \frac{\omega^2}{2}r^2\,. \tag{4}$$

Both the macromotion and micromotion of a single ion in the potential well are completely described by the macromotion frequency parameter ω.

If the well contains a large number of ions, the effective potential is modified by the ionic space-charge. The total effective potential seen by an ion is then given by

$$\Phi_{\text{tot}}(\mathbf{r}) = \Phi(\mathbf{r}) + q\Phi_q(\mathbf{r})\,, \tag{5}$$

where the electric space charge potential Φ_q is related to the ionic number density $n(r)$ by Poisson's equation. Assuming the ion cloud has statistically thermalized at a temperature T, the ion number density will satisfy a Boltzmann distribution,

$$n(r) = C' \exp(-E_{\text{tot}}/k_B T) \tag{6}$$

with

$$E_{\text{tot}} = \tfrac{1}{2}mv^2 + \Phi_{\text{tot}}(r)$$

and C' a normalization constant. The statistically independent momentum (velocity) distribution can be integrated out, leaving

$$n(r) = C \exp[-\Phi_{\text{tot}}(r)/k_B T]. \tag{7}$$

Solving for $\Phi_{\text{tot}}(r)$ in terms of $n(r)$, and using the Poisson equation gives a nonlinear second-order equation for $n(r)$:

$$n'' - \frac{n'^2}{n} + 2\frac{n'}{r} - \frac{n^2 q^2}{\varepsilon_0 k_B T} + \frac{3m\omega^2 n}{k_B T} = 0 \tag{8}$$

with the constraint

$$\int n(r) d^3 r = N, \tag{9}$$

where N is the total number of ions. Equation (8) can be easily solved in the following two limits:

$$n(r) = \frac{3m\omega^2 \varepsilon_0}{q^2}, \quad [r \leqq (Nq^2/4\pi m\omega^2 \varepsilon_0)^{1/3}],$$
$$\text{for} \quad T \to 0$$
$$n(r) = (\text{const}) \exp\left(-\frac{3m\omega^2 r^2}{2k_B T}\right) \quad \text{for} \quad T \to \infty. \tag{10}$$

Note that for low temperatures the cloud condenses to a uniform distribution which has a space charge generated potential that precisely cancels the effective trapping potential within the cloud. At high temperatures the ions see a negligible space charge effect and satisfy a Boltzmann distribution with respect to the trapping fields.

For a given set of trapping parameters, (8 and 9) can be numerically solved. Figure 1 illustrates the charge distributions for several temperatures with fixed trap parameters and ion number. Mass 199, $N = 2 \times 10^6$, and $\omega/2\pi = 50$ kHz have been chosen to correspond to the conditions used in [10]. Figure 2 shows the normalized total effective potential derived from these charge distributions using (7) in the form

$$\Phi_{\text{tot}}(r) = -k_B T \ln\left(\frac{n(r)}{n(o)}\right), \tag{11}$$

where the potential has been set equal to zero at the cloud center.

Note that at low temperatures the potential tends to approximate a spherical square well. Under typical conditions it may be assumed that the densities of ions, neutrals and background gas atoms are such that the rate of collisions of the ions with the potential barrier at the cloud edge is much greater than the rate of ion-ion, ion-neutral, or ion-light gas collisions. Thus, the ion trajectories will roughly correspond to free rectilinear paths in the cloud interior, with rather sharp specular reflection at the relatively well-defined cloud surface. Also, the total potential is taken to be spherically symmetric implying orbital angular momentum conservation, and therefore the ion trajectories remain in planes that contain the trap center.

The intuitive picture of the ion macromotion trajectories at this point is that of ions bouncing around inside a hollow rigid sphere defined by the total potential. However as can be seen from Fig. 2, the potential is not precisely defined by a rigid sphere (except at $T = 0$), but rather a potential well with

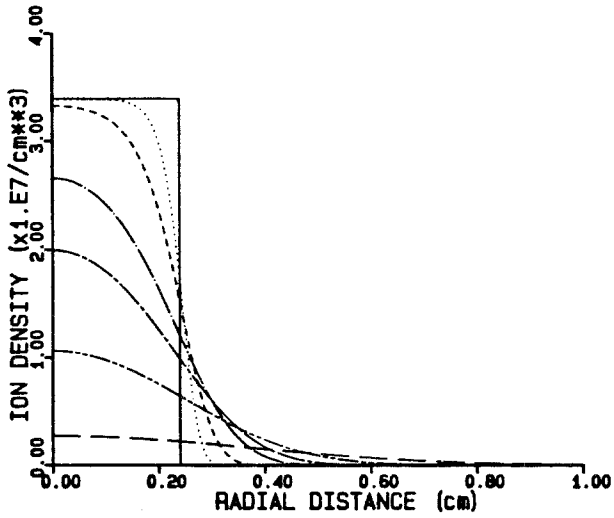

Fig. 1. Ion density as a function of radial distance for several different input temperatures, with $N = 2 \times 10^6$ ions and $\omega/2\pi = 50$ kHz. (The curves are, from top to bottom: $T = 0$, 300, 1000, 3000, 5000, 10,000, and 30,000 K)

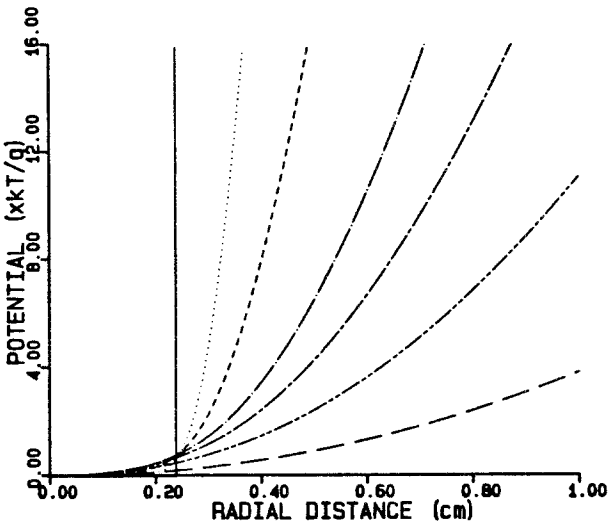

Fig. 2. The total effective potential as a function of radial distance for several different input temperatures, with $N = 2 \times 10^6$ ions and $\omega/2\pi = 50$ kHz. (Same temperatures as Fig. 1)

extended "soft" walls. Therefore, for a given initial ion position and velocity we must solve for the precise trajectory using the numerical values of the potential given by (11). The equation for the ion two-dimensional trajectory in the plane defined by the initial velocity vector and the trap center can be written in terms of two integrals

$$\Theta = \int_{r_0}^{r} \frac{dr}{r^2 \sqrt{\frac{2mE}{l^2} - \frac{2mV(r)}{l^2} - \frac{1}{r^2}}}$$
$$t = \int_{r_0}^{r} \frac{dr}{\sqrt{\frac{2}{m}[E - V(r) - l^2/2mr^2]}}, \tag{12}$$

where Θ and t are the angle and time elapsed as the ion travels from r_0 to r, E, and l are the ion energy and angular momentum, and $V(r)$ is the ion total potential energy. These equations can be numerically integrated for arbitrary ion initial conditions and potential.

In summary, given the ion trapping parameters defined in (1), the ion number N, and a temperature T, the ion number density can be computed. From this the total potential seen by the ions can be determined, and thus the ion trajectory for an arbitrary initial ion velocity and position.

2. Asymptotic Estimation of the Doppler Sideband Frequencies

The Doppler sideband frequencies can be estimated simply for the cases of very high and very low temperatures. At very high temperatures the macromotion amplitude is large so the density of the stored ion cloud is low, and the space charge effects are unimportant. The total potential seen by the ions is therefore the quadratic pseudopotential given by (3). In the case of spherical symmetry the ion macromotion is thus simple harmonic motion in three dimensions at the angular frequency ω given by (3). As described in the introduction, this motion will cause the observed hyperfine spectrum to show narrow sidebands at $\pm\omega/2\pi$ and harmonics. A reduced sideband frequency F^* can be defined by

$$F^* = 2\pi f_{SB}/\omega, \tag{13}$$

where f_{SB} is the Fourier frequency in Hz of the first-order Doppler sideband. At sufficiently high temperatures we expect $F^*_{hot} \approx 1$ for all values of the parameters m, ω, and N. These sidebands will of course be accompanied by sidebands at the micromotion frequency $\Omega/2\pi$ and its harmonics.

At very low temperatures the situation is different. As described in Sect. 1, the total potential is strongly modified by the space charge of the ion cloud, and is approximately a spherical square well with a radius r_0 given by (10). The orbit periods for ions with velocity v lie between the limits $4r_0/v$ and $2\pi r_0/v$ corresponding to diametric and equatorial orbits, respectively. The appropriate average ion velocity must be close to the most probable thermal velocity v_{mp} for the Maxwell distribution given by

$$v_{mp} = (2k_B T/m)^{1/2}. \tag{14}$$

The reduced frequency of maximum sideband intensity will thus be given by

$$F^*_{cold} = v_{mp}/\gamma r_0 \omega,$$

where

$$2/\pi < \gamma < 1. \tag{15}$$

The value of γ represents the geometrical average in phase space over all possible orbits, which should be independent of m, ω, N, and T. Substituting the values of r_0 and v_{mp} gives

$$F^*_{cold} = \gamma^{-1}(T^*)^{1/2}, \tag{16}$$

where we have defined a reduced temperature

$$T^* = T/T_0,$$

with

$$T_0 = m^{1/3}(q^2\omega N/4\pi\varepsilon_0)^{2/3}/2k_B.$$

Thus at sufficiently low temperature we expect F^* to be given in terms of the parameters m, ω, N, and T by (16), and at sufficiently high temperatures we expect $F^* \approx 1$.

It is instructive to notice that the characteristic temperature T_0 of the low temperature motion is related to $\Phi(r_0)$, the pseudopotential at the edge of the cold cloud, by $k_B T_0 = \Phi(r_0)$. Thus for $T^* \approx 1$ the cold cloud model might be expected to break down. The practical significance of the reduced temperature T^* will become apparent when the results of rigorous calculations are considered in Sect. 4.

3. Complete Calculation of Sideband Spectra

As established in Sect. 1, the trapped ions have a thermal macromotion following calculable two-dimensional trajectories governed by the effective potential. In a frequency standard, these ions would be irradiated by microwave traveling waves at the hyperfine frequency. The macromotion causes the ions to see the microwaves with an additional position and time dependent phase factor. We assume an ion with position $\mathbf{r}(t)$ sees a plane wave microwave field

$$B(t) = B_0 \cos[\omega_0 t - \mathbf{k}\cdot\mathbf{r}(t) + \phi], \tag{17}$$

where B_0 is the peak field strength, ω_0 and $\mathbf{k}$ are the microwave angular frequency and wave vector, and ϕ is an arbitrary phase factor due to the random starting phase of the incident wave. The power spectral density of the radiation perceived by the ions is given by the Fourier transform of the autocorrelation function of the field. If the following reasonable assumptions are made: i) that the radiation in the sidebands is incoherent, and ii) that transitions do not change the populations of the hyperfine levels significantly, the induced transition rate will be proportional to the power spectral density of the observed radiation. The shape of the observed Doppler sidebands will thus be that of the power spectral density. The power spectral density $P(\omega)$ of the field of (17) is given by

$$P(\omega)=4\int_0^\infty d\tau \Psi(\tau)\cos(\omega\tau), \tag{18}$$

where $\Psi(\tau)$ is the autocorrelation function given by

$$\Psi(\tau)=B_0^2\langle\cos\{\omega_0(t+\tau)-\mathbf{k}\cdot\mathbf{r}(t+\tau)+\phi\}\cdot\cos\{\omega_0 t-\mathbf{k}\cdot\mathbf{r}(t)+\phi\}\rangle, \tag{19}$$

where the brackets signify averaging over an adequate statistically weighted ensemble of ion trajectories. We also note that $\Psi(\tau)$ is independent of t in (19) since $B(t)$ is a statistically stationary variable. Averaging over the random phase factor ϕ eliminates the explicit t dependence and yields for $\Psi(\tau)$

$$\Psi(\tau)=\frac{B_0^2}{2}\mathrm{Re}\{e^{i\omega_0\tau}\langle e^{-i\mathbf{k}\cdot\Delta\mathbf{r}(\tau)}\rangle\}, \tag{20}$$

where $\Delta\mathbf{r}(\tau)=\mathbf{r}(\tau)-\mathbf{r}(0)$. The ensemble average of the bracketed expression must be done to compute $\Psi(\tau)$, which is then used to compute the power spectrum via (18). However, the three-dimensional rotational invariance of the potential which governs the ion trajectories can be further exploited to simplify (20). The argument is as follows. In a time interval τ, an ion will trace out a two-dimensional trajectory segment whose chord is $\Delta\mathbf{r}(\tau)$. Due to rotational invariance, within the ion statistical ensemble it is equally probable that there is an ion with a trajectory segment whose chord yields a $\Delta\mathbf{r}(\tau)$ rotated by any angle in the parameter manifold of the three-dimensional rotating group. Thus we can sum (average) over all orientations of $\Delta\mathbf{r}(\tau)$ integrating over the full 4π solid angle

$$\langle e^{-i\mathbf{k}\cdot\Delta\mathbf{r}(\tau)}\rangle=\langle\int e^{-ik\Delta r\cos\Theta}\sin\Theta d\Theta\rangle=2\left\langle\frac{\sin[k\Delta r]}{[k\Delta r]}\right\rangle. \tag{21}$$

The simplified expression for $\Psi(\tau)$ is then

$$\Psi(\tau)=B_0^2\cos(\omega_0\tau)\left\langle\frac{\sin[k\Delta r(\tau)]}{[k\Delta r(\tau)]}\right\rangle. \tag{22}$$

The autocorrelation function and thus the power spectral density for absorption of microwave radiation by the trapped ions can now be computed using the statistical sampling techniques of Monte Carlo programming. The procedure to compute the autocorrelation function of (22) is the following. The trapping parameters defined in (1), the total number of trapped ions and the temperature T of the thermalized ion cloud, are chosen. From this information, the ion number density $n(r)$ and the effective total potential $\Phi_{\mathrm{tot}}(r)$ seen by the ions can be computed. Statistically generated ion trajectories can be calculated, and their contributions to $\Psi(\tau)$ can be determined from equation (22). The iterated algorithm is the following:

1) Generate a starting point for an ion trajectory from the rotationally symmetric spatial probability function

$$P_1(r)dr=n(r)r^2dr. \tag{23}$$

2) Generate an initial speed for the ion from the Maxwell-Boltzmann thermalized distribution

$$P_2(v)dv=\exp(-mv^2/2kT)v^2dv. \tag{24}$$

3) Generate an initial velocity direction given by the angle Θ from an arbitrarily defined z-axis

$$P_3(\Theta)d\Theta=\sin(\Theta)d\Theta. \tag{25}$$

4) Compute the trajectory using (12). Computation time is minimized by computing one full trajectory segment from $r_{\min}$ to $r_{\max}$ and reflecting this reproduced segment repeatedly about the appropriate axes of symmetry. [Also, analytic expressions for the integrals near the turning points must be used because of the integrable singularities in (12).]

5) Compute the contribution to the autocorrelation function using (22). Loop back to Step 1.

After computing an appropriate number of statistically generated contributions to the autocorrelation function, the absorption power spectral density can be computed using (18). This process can be repeated for various cloud temperatures and the resultant spectral densities compared with the measured data. In this way, the temperature of the physical experimental cloud can be determined, and the consistency of the thermalized ion cloud model investigated.

As will be seen in the next section, very good results have been achieved. However, it is of interest to investigate possible corrections to our model. The largest correction expected would be the inclusion of ion-ion scattering as the ions follow their trajectories through the cloud interior. This scattering would manifest itself as a slowly growing deviation from the unscattered trajectory due to multiple Coulomb scattering, and would give a finite lifetime to any distinct

orbit. This process was found to have a negligible effect upon the results, and is thus relegated to discussion in the appendix.

4. Results of Calculation

The formalism of the previous sections can now be used to compute the effects of ion thermal macromotion on the power spectral density of microwave radiation seen by trapped ions. As stated in the introduction, the phase modulated signal seen by the ions is a Dicke spectrum consisting of an unshifted carrier and first-order Doppler sidebands uniformly spaced by the motional modulation frequency. What will be computed here is the single-sided power spectral density of the first-order Doppler sidebands, which will be plotted as a function of the frequency difference from the unshifted carrier.

In order to calculate the ion density distribution it is necessary to choose values of the ion mass m, the trapping parameter ω, the total number of ions N, and the temperature T. To complete the calculation of the sideband spectra, a value of the wavelength λ at the hyperfine frequency is also required.

Figure 3 shows the results of typical calculations for trapped ^{199}Hg ions. The autocorrelation function is plotted for various temperatures, suppressing the baseline due to the unshifted carrier, together with the corresponding power spectra. For comparison with the experimental data [10, 13] the parameter values $m = 3.329 \times 10^{-25}$ kg $\omega/2\pi = 50$ kHz, $N = 2 \times 10^6$, and $\lambda = 7.5$ mm have been used.

The following general observations can be made on these results:

1) The frequency of the first maximum in the sideband intensity is a monotonically increasing function of temperature.

2) The first maximum falls well below $\omega/2\pi$ at low temperatures and asymptotically approaches this value at high temperatures, as predicted by the simple analysis of Sect. 2.

3) Sidebands occur at harmonics of the frequency of the first maximum. This is particularly obvious at high temperatures, where the cloud is largest and the condition $2\pi r/\lambda \approx 1$ is approached. Figure 4 shows a power spectral density plotted up to 200 kHz showing this effect.

4) The width of the first-order sidebands decreases uniformly with increasing temperature, as expected from the fact that the effective potential becomes more nearly harmonic.

5) At higher temperatures, there is a small peaked contribution to the spectral density at low frequencies (1–10 kHz). Detailed analysis of individual trajectories has revealed that this originates in the fact that general

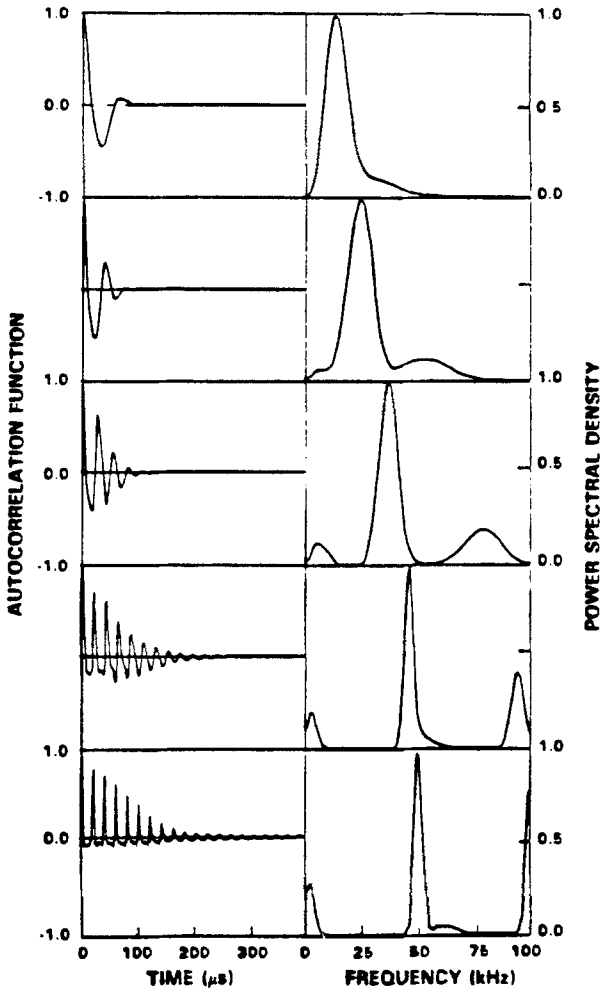

Fig. 3. Computed autocorrelation functions and resultant power spectral densities for various input temperatures. ($N = 2 \times 10^6$ ions $\omega/2\pi = 50$ kHz, and from top to bottom: $T = 300$, 1000, 3000, 10,000, and 30,000 K)

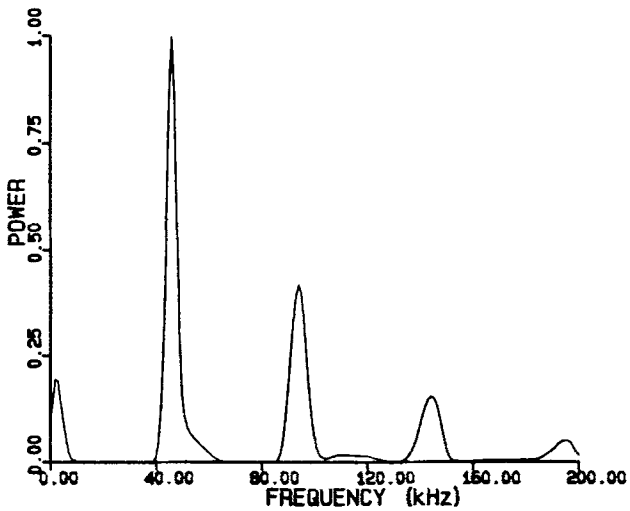

Fig. 4. Computed power spectral density plotted to 200 kHz to exhibit higher harmonics of the first-order Doppler sideband. ($N = 2 \times 10^6$ ions, $\omega/2\pi = 50$ kHz, $T = 10{,}000$ K)

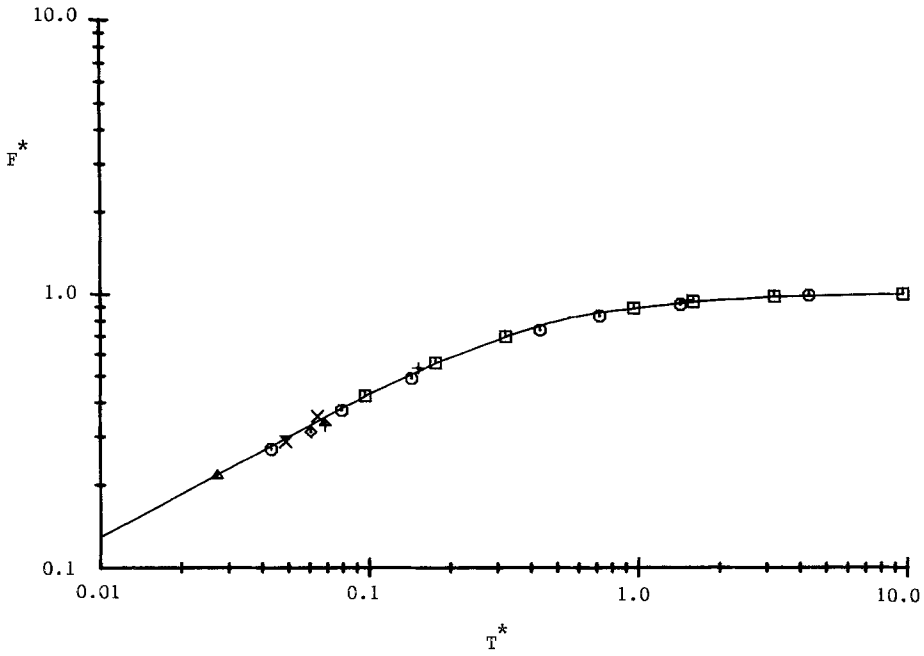

Fig. 5. The reduced frequency F^* of the maximum intensity of the first order Doppler sideband vs. the reduced temperature T^*, calculated for various values of m, ω, and N. ($m=3.329\times10^{-25}$ kg, $\omega/2\pi=50$ kHz: □: $N=0.6\times10^6$ ions; ⊙: $N=2\times10^6$ ions; ▲: $N=4\times10^6$ ions; +: $N=0.3\times10^6$ ions; ×: 1.1×10^6 ions. $N=2\times10^6$ ions, $\omega/2\pi=30$ kHz: ↑: $m=3.329\times10^{-25}$ kg, ×: $m=2.292\times10^{-25}$ kg)

orbits are not closed, and the "orbital symmetry lines" defined by the orbital turning points have a precessional motion superposed upon the higher frequency orbital motion. This low frequency precession manifests itself through the phase nonlinearity of the autocorrelation function.

In order to demonstrate the systematics of the variation of the sideband frequencies we show in Fig. 5 the results of plotting the frequency of the maximum intensity of the first-order sideband in the calculated spectra (divided by $\omega/2\pi$) against the calculated value of the reduced temperature T^* defined in (16). The calculations have been extended to several different values of m, ω, and N as shown in the figure caption. A surprising and useful result is seen to be that, for the data calculated, the values of F^* appear to be given by a single function of T^* for all the parameter values chosen. At low temperatures the rigorously calculated results fall within the limits given by the simple theory in (16). At high temperatures F^* approaches unity. The calculated results are quite well described by the phenomenological relationship

$$F^*=[1+0.32(T^*)^{-2}]^{-1/4},$$

implying a value of $\gamma=0.75$.

The data shown in Fig. 5 demonstrates that the position of the first-order sideband can be used to estimate the ion cloud temperature as long as the reduced temperature T^* is smaller than about 0.5. The estimate requires that the values of m, ω, and N be known with sufficient accuracy.

Jardino et al. [17] have found using the same method of calculation as that discussed above that the sideband frequency is independent of temperature for a given density, $n(0)$, of ions at the center of the trap. For this result to be compatible with our finding that F^* is a single-valued function of T^*, $n(0)$ must itself be a single-valued function of T^*. For given values of m and ω, (16) shows that for a constant $n(0)$, the relationship $T\propto N^{2/3}$ must hold. Our calculated density distributions for $m=3.329\times10^{-25}$ kg and $\omega=2\pi\times50$ kHz do indeed demonstrate this unexpected result for values of N between 10^6 and 5×10^6 ions, and thus there is no disagreement between our results and those of Jardino et al. [17].

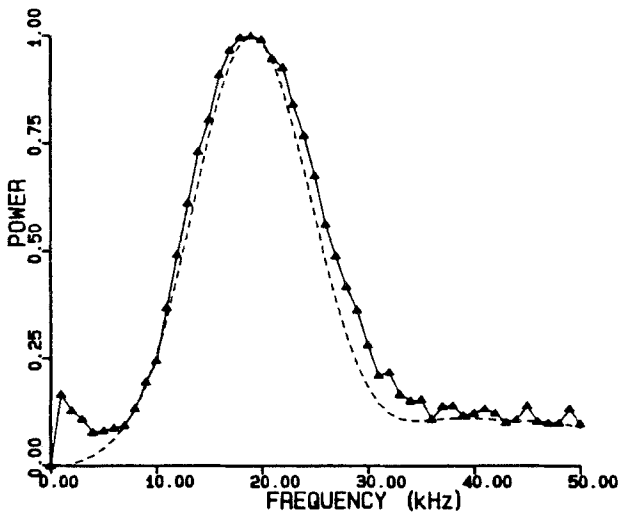

Fig. 6. Measured (solid) and theoretical (dashed) power spectral densities as a function of frequency away from the carrier frequency. ($N=2\times10^6$ ions, $\omega/2\pi=50$ kHz, and the input temperature $T=564$ K as determined from Fig. 5)

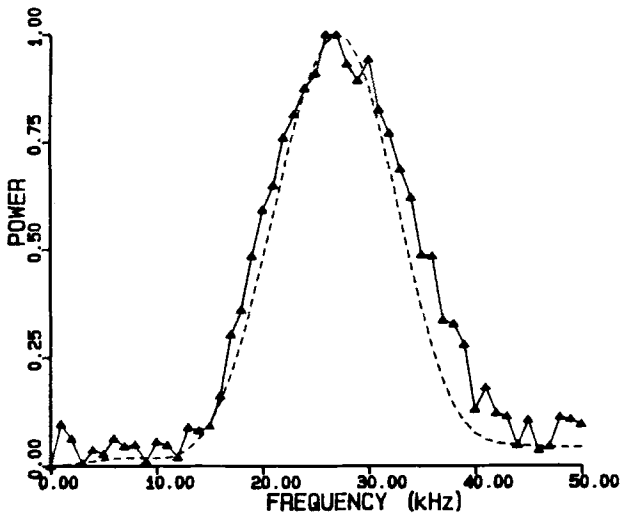

Fig. 7. Measured (solid) and theoretical (dashed) power spectral densities as a function of frequency away from the carrier frequency. ($N=0.6\times10^6$ ions, $\omega/2\pi=50$ kHz, and the input temperature $T=503$ K as determined from Fig. 5)

5. Comparison with Experiment

Measurements of the first-order Doppler sidebands in a mercury-199 trapped ion frequency standard have been published elsewhere [13]. Figures 6 and 7 show the results of fitting calculated spectra using the macromotion temperature T as determined from Fig. 5. The experimental data appear to be reasonably well accounted for by quite similar temperatures.

The intensity at low Fourier frequencies in the measured data is probably the edge of the central line which is saturated and broadened by the relatively high microwave intensity necessary to see the sidebands.

6. Conclusions

A self-consistent model for a cloud of ions in an rf quadrupole trap has been analyzed, and the first-order Doppler sideband lineshapes calculated from the autocorrelation function of the motion. We find unexpectedly that the first-order sideband frequency is given quite accurately by a single-valued function of a reduced temperature depending on m, ω, N, and T.

It follows that, for a reasonably cold ion cloud, the effective temperature can be easily estimated from the position of the measured first-order Doppler sidebands of the Dicke spectrum, as long as the parameters m, ω, and N are known.

Knowledge of the temperature implies a knowledge of the ion spatial distribution and also the ion thermal speed distribution.

These quantities are necessary to determine the second-order Doppler corrections to the center frequency of the ion trap frequency standard due to ion micromotion and macromotion, respectively. Our confidence in previous estimates of the second-order Doppler shift for trapped mercury ions [10, 13] is increased by the excellent agreement between the rigorous calculations of the sideband frequencies, and the predictions of the simple model of the cold cloud which was used to calculate the second-order Doppler shift.

Appendix

As stated in Sect. 3, the primary correction to our model would be the approximate inclusion of ion-ion scattering as the ions follow their trajectories through the cloud interior. The effect of this multiple Coulomb scattering would be a slowly growing (randomized) deviation from the unscattered trajectory, which would introduce a randomized phase modulation to the microwave radiation frequency seen by the ion. We incorporate this scattering off-set by adding a contribution to the ion trajectory displacement vector

$$\Delta\mathbf{r}(\tau)\to\Delta\mathbf{r}(\tau)+\boldsymbol{\varepsilon}(\tau), \tag{A.1}$$

where $\boldsymbol{\varepsilon}(\tau)$ is a vector transverse to the ion trajectory and is weighted by a distribution governed by the scattering dynamics. The distribution is a function of the density of ions, velocity and mass of the ions, and τ. As τ becomes larger, we expect the width of the transverse distribution to grow due to the increased number of scatterings. We further expect it to grow in a fashion analogous to a statistical random walk.

Inclusion of the multiple Coulomb scattering effect in the autocorrelation function of Sect. 3 changes (17) to the following simple form

$$\Psi(\tau)=\frac{B_0^2}{2}\mathrm{Re}\{e^{i\omega_0\tau}\langle e^{-i\mathbf{k}\cdot\Delta\mathbf{r}(\tau)-i\mathbf{k}\cdot\boldsymbol{\varepsilon}(\tau)}\rangle\}, \tag{A.2}$$

where the brackets denote averaging over the distribution in the scattering off-set $\boldsymbol{\varepsilon}$, in addition to the usual averaging over the statistical ensemble.

The direction of $\boldsymbol{\varepsilon}$ is orthogonal to the ion trajectory and randomized in this plane. Here we will outline the derivation of the probability distribution for the magnitude of $\boldsymbol{\varepsilon}$. The orthogonal distance ε away from the unperturbed trajectory is given by

$$\varepsilon(\tau)=\int_0^t v_\perp(t')dt', \tag{A.3}$$

where $v_\perp(t)$ is the velocity orthogonal to the unperturbed trajectory generated by scattering. The velocity $v_\perp(t)$ can be rewritten as $[v\sin\Theta(t)]$, where $\Theta(t)$ is the angle of deviation from the unperturbed trajectory and v is the (constant) ion velocity

$$\varepsilon(\mathrm{t})=\mathrm{v}\int_0^t\sin[\Theta(t')]dt'. \tag{A.4}$$

To characterize the distribution $\Theta(t)$ we model the scattering as that of an ion of velocity v passing through a cloud of effectively stationary ions, and undergoing multiple Coulomb scattering. The scattering cross-section for a single ion-ion scattering is the simple Rutherford cross-section

$$\frac{d\sigma}{d\Omega}=\tfrac{1}{4}\left(\frac{e^2}{4\pi\varepsilon_0 mv^2}\right)^2\frac{1}{\sin^4\Theta/2}. \tag{A.5}$$

As is always the case with the naive application of this formula, there is an apparent infra-red ($\Theta \to 0$) singularity. However it is known from physical considerations that there is a $\Theta_{\min}$ and a $\Theta_{\max}$ for the process under consideration. To determine $\Theta_{\min}$ we simply note that for small angle scattering momentum conservation gives $\Delta\Theta \approx e^2/2\pi\varepsilon_0 bmv^2$, where b is the scattering impact parameter. For the scattering of a screened charge (analogous to Debeye screening), there is a maximum impact parameter and thus a minimum $\Delta\Theta$. The screening here comes from the compensating motion of the "spectator" ions which move to keep the long range potential gradients inside the cloud equal to zero. The magnitude of b is estimated to be always less than 2–3 interionic distances in the cloud interior, which leads to

$$\Delta\Theta_{\min} \approx \frac{e^2}{2\pi\varepsilon_0 \eta r_0 mv^2}, \tag{A.6}$$

where $\eta \approx 2$–3, r_0 is the inter-ionic distance given by $r_0 = (3/4\pi n)^{1/3}$, and n is the ion number density.

Similarly, there is a $\Delta\Theta_{\max}$. This originates from the fact that the ions are extended objects of distributed charge. As a result, the scattering cross-section falls substantially below the Rutherford expression for large angles due to diffraction effects. The scattering is confined to angles $\lesssim(\lambda/2\pi R)$, where λ is the ion de Broglie wavelength and R is the ion radius. For wider angles the wavelets from different parts of the scatterer destructively interfere. Using $p = \hbar k = 2\pi\hbar/\lambda$ the expression for $\Delta\Theta_{\max}$ becomes

$$\Delta\Theta_{\max} \approx \frac{\hbar}{mvR}. \tag{A.7}$$

Given (A.5–7), the mean squared angle can be computed for a single collision

$$\langle\Theta^2\rangle = \int \Theta^2 \frac{d\sigma}{d\Omega} \Big/ \int \frac{d\sigma}{d\Omega} d\Omega$$
$$\approx 2\Theta_{\min}^2 \ln(\Theta_{\max}/\Theta_{\min}). \tag{A.8}$$

Since successive collisions are independent events, the central limit theorem of statistics implies that for a large number of collisions N, the distribution in angle will be approximately Gaussian around the forward direction with a mean square angle

$$\langle\theta^2\rangle = \langle\Theta^2\rangle. \tag{A.9}$$

Using the expression for the total number of collisions after time t

$$N(t) = n\sigma_{\text{Tot}} vt, \tag{A.10}$$

the final expression becomes

$$\langle\theta^2\rangle = 2\pi n \left(\frac{e^2}{2\pi\varepsilon_0 mv^2}\right)^2 \ln(\Theta_{\max}/\Theta_{\min})\, vt. \tag{A.11}$$

Equation (A.11) for the RMS angle of scattering can be used to compute the RMS value of ε using (A.4):

$$\varepsilon_{\text{RMS}}(\tau) = Ct^{3/2} \tag{A.12}$$

where

$$C \equiv \tfrac{2}{3}\left[2\pi n \left(\frac{e^2}{2\pi\varepsilon_0 mv^2}\right)^2 \ln(\Theta_{\max}/\Theta_{\min})\right]^{1/2} v^{3/2}.$$

As before, the central limit theorem gives a Gaussian probability distribution in the parameter ε

$$P(\varepsilon)d\varepsilon = \sqrt{\frac{2}{C^2 t^3 \pi}} \exp\left(-\frac{\varepsilon^2}{2C^2 t^3}\right) d\varepsilon. \tag{A.13}$$

This weighting function is used in (A.2) after the angular averaging of ε is completed. The expression for the autocorrelation function of (A.2) including ion-ion scattering can be reduced to

$$\Psi(\tau) = \left\langle \frac{B_0^2}{2} \mathrm{Re}\{e^{i\omega_0 t}\langle e^{-i\mathbf{k}\cdot\Delta\mathbf{r}(\tau)}\rangle \cdot \left[\int_0^1 \exp\left(-\frac{C^2k^2\tau^3\alpha^2}{2}\right) d\alpha\right]\right\rangle. \tag{A.14}$$

This is the same as the original unperturbed autocorrelation function of (20), modified by the scattering term in brackets which tends to damp the correlation for large τ. As an estimate of the importance of this effect, putting in typical values of the velocity and density of Hg ions in the ^{199}Hg frequency standard yields a scattering induced damping time on the order of a half millisecond. As seen in the results of Sect. 3, the autocorrelation function has already become extremely damped on a much shorter time scale from the statistical ensemble average, and this scattering effect is normally negligible. The only situation where it may have a modest effect is when the cloud is extremely hot, and the damping of the autocorrelation function from the statistical ensemble average is of comparable time.

References

1. H.G. Dehmelt: Adv. At. Mol. Phys. **5**, 109 (1969)
2. H.G. Dehmelt: Adv. At. Mol. Phys. **3**, 53 (1967)
3. F.L. Walls, G.H. Dunn: Phys. Today **27**, 30 (August 1974)
4. H.A. Schuessler, E.N. Fortson, H.G. Dehmelt: Phys. Rev. **187**, 5 (1969)
5. F.G. Major, G. Werth: Phys. Rev. Lett. **23**, 1155 (1973)
6. D.J. Wineland: Proc. 11th Annual PTTI Appl. & Planning Meeting (1979), NASA Confg. Publ. 2129, p. 81
7. D.J. Wineland, W.M. Itano, J.C. Bergquist, F.L. Walls: Proc. 35th Annual Symposium on Frequency Control (1981), Electronic Industries Assoc., p. 602
8. M. Jardino, M. Desaintfuscien, R. Barillet, J. Viennet, P. Petit, C. Audoin: Appl. Phys. **24**, 107 (1981)
9. D.J. Wineland: Proc. 13th Annual PTTI Appl. & Planning Meeting (1981). NASA Conf. Publ. 2220, p. 579
10. L.S. Cutler, R.P. Giffard, M.D. McGuire: Proc. 37th Frequency Control Symposium (1983), p. 32
11. J.J. Bollinger, W.M. Itano, D.J. Wineland: Proc. 37th Frequency Control Symposium (1983), p. 37
12. H. Schaaf, V. Schmeling, G. Werth: Appl. Phys. **25**, 249 (1981)
13. L.S. Cutler, R.P. Giffard, M.D. McGuire: Appl. Phys. B**36**, 137–142 (1985)
14. R.D. Knight, M.H. Prior: J. Appl. Phys. **50**, 3044 (1979)
15. R.D. Knight: PhD Thesis: Univ. of California, Berkeley (1979)
16. R.H. Dicke: Phys. Rev. **89**, 472 (1953)
17. M. Jardino, F. Plumelle, M. Desaintfuscien, J.L. Duchene: Proc. 38th Annual Symposium on Frequency Control (1984) IEEE Press. 84CH2062-8, p. 431